



Published in final edited form as:

*Cell Mol Bioeng.* 2011 March 1; 4(1): 9–27. doi:10.1007/s12195-010-0142-y.

## Effects of Morphology vs. Cell–Cell Interactions on Endothelial Cell Stiffness

**Kimberly M. Stroka and Helim Aranda-Espinoza**

Fischell Department of Bioengineering, University of Maryland, College Park, 3138 Jeong H. Kim Engineering Building, College Park, MD 20742, USA

### Abstract

Biological processes such as atherogenesis, wound healing, cancer cell metastasis, and immune cell transmigration rely on a delicate balance between Cell–Cell and cell–substrate adhesion. Cell mechanics have been shown to depend on substrate factors such as stiffness and ligand presentation, while the effects of Cell–Cell interactions on the mechanical properties of cells has received little attention. Here, we use atomic force microscopy to measure the Young's modulus of live human umbilical vein endothelial cells (HUVECs). In varying the degree of Cell–Cell contact in HUVECs (single cells, groups, and monolayers), we observe that increased cell stiffness correlates with an increase in cell area. Further, we observe that HUVECs stiffen as they spread onto a glass substrate. When we weaken Cell–Cell junctions (i.e., through a low dose of cytochalasin B or treatment with a VE-cadherin antibody), we observe that cell–substrate adhesion increases, as measured by focal adhesion size and density, and the stiffness of cells within the monolayer approaches that of single cells. Our results suggest that while morphology can roughly be used to predict cell stiffness, Cell–Cell interactions may play a significant role in determining the mechanical properties of individual cells in tissues by careful maintenance of cell tension homeostasis.

### Keywords

Cell mechanics; Cell spreading; Focal adhesions; Cell tension; Actin

## INTRODUCTION

The mechanical properties of cells are important contributors to the health of a tissue, and a pathological state can sometimes be determined by measuring the stiffness of cells or tissues.<sup>8,10</sup> For example, arteries stiffen during the progression of atherosclerosis<sup>47</sup> and tissues stiffen in cancer.<sup>55</sup> In the case of arteries, the mechanical properties of endothelial cells (ECs) are affected by many factors, including substrate stiffness, substrate ligands, shear stress, and the presence of soluble molecules. In a recent review on the biophysics of leukocyte transmigration, Stroka and Aranda-Espinoza summarize various *in vitro* treatments and conditions which affect endothelial cell stiffness.<sup>69</sup> While it has been widely recognized that it is important to study the mechanical properties of cells, much of the published work regarding cell stiffness focuses on single cells. Though this simplifies the experimental system, it is not always physiological, since, for example, ECs exist as a monolayer at the luminal surface of blood vessels. In this state, the cells are exposed to

many neighbors in close contact, and the junctions are lined with many different molecules which bind the cells together,<sup>22</sup> one of which is vascular endothelial (VE)-cadherin. VE-cadherin is a homophilic protein which localizes to cellular junctions, physically links to F-actin, and plays an important role in both mechanical<sup>20,41,42,65</sup> and biochemical signaling<sup>24,39,43</sup> pathways. Due to their role as mechano-sensors, cadherins have been suggested as targets for cancer therapy<sup>9</sup>; further, interactions between cadherins, actin, and myosin can create the forces necessary for wound closure.<sup>1</sup> While there are many proteins which localize at Cell–Cell junctions, this manuscript focuses on VE-cadherin due to its linkage with the actin cytoskeleton, an interaction which seems to be very relevant to tension homeostasis and cell stiffness.

Cell–Cell interactions play a critical role in angiogenesis and endothelial homeostasis. As cells gain neighbors during monolayer formation, their morphology changes drastically, and it is known that cell geometry plays a significant role in regulating homeostasis of a cell.<sup>16</sup> Despite the occurrence of contact inhibition<sup>25,49,50</sup> in a monolayer, ECs do have the ability to reorganize themselves, but it is likely a different process than what occurs in single cells. While single cells are able to move freely, with constraints only due to adhesion with the substrate and cytoskeletal remodeling, cells in a monolayer are constrained by Cell–Cell adhesions as well as cell–substrate adhesions.<sup>44</sup>

Cell mechanical properties, specifically, traction force generation, have been shown to depend on the presence of neighbors. Cell traction forces increase when two cells come in contact.<sup>15</sup> Further, two cells are able to communicate mechanically with each other when grown on soft, flexible substrates.<sup>59</sup> There is also evidence that cells maintain tension through Cell–Cell junctions<sup>26,72</sup> and are able to communicate mechanically during collective cell migration.<sup>71</sup> However, we do not know how Cell–Cell interactions affect cell stiffness, nor do we fully understand how cells communicate mechanically in a monolayer. As mentioned above, such changes in cell stiffness might affect important physiological functions, such as immune cell transmigration, atherogenesis, and cancer cell metastasis.

Our study uses atomic force microscopy (AFM) to measure the Young's modulus of live human umbilical vein endothelial cells (HUVECs). AFM is a useful tool for measuring the response of cells to an applied force, from which the Young's modulus can be calculated. Hoffman and Crocker provide an extensive review on the response of cells to applied forces and a summary of different tools for measuring those responses.<sup>34</sup> AFM imaging can further be used to obtain topographical information about a sample. Previously, AFM has been used to quantify the Young's modulus of many cell types. For example, for ECs specifically, AFM has been used to determine the effects of environmental conditions such as oxidized low density lipoprotein,<sup>17</sup> potassium,<sup>53</sup> plasma sodium,<sup>54</sup> and substrate stiffness<sup>12</sup> on cell stiffness. For soft samples such as cells, the Hertz–Sneddon model has often been used to determine Young's modulus from AFM force–distance curves (for review see Vinckier and Semenza<sup>73</sup>), and AFM cantilevers with spherical probes have been used to minimize exerted traction on the cells. The Hertz–Sneddon model<sup>66</sup> represents cells as isotropic, linearly elastic half-spaces and holds when deformations are small. It assumes an infinitely hard tip which is much stiffer than the deformable sample, and it can also account for the geometry of the tip. These assumptions can be made under our experimental conditions, and thus the Hertz–Sneddon model is appropriate to use in our case. Further details on the theoretical basis for this model can be found in several references.<sup>66,70,79</sup>

Here, we combine AFM imaging with force measurements on live cells to obtain a topographical map which contains local measurements of Young's modulus at specific locations. We measure both Young's modulus and area of spreading cells and find that cell stiffness increases with spreading area. Then, we measure the area and stiffness of single

cells, groups, and monolayers and find that morphology can roughly be used to predict cell stiffness, though monolayers are stiffer than expected based on cell area. However, when F-actin is significantly disrupted using a high dose of cytochalasin B (cytoB), we observe drastic cell rounding, as previously reported,<sup>62,75</sup> and the stiffness of the cells softens to the measured value based on spreading area. When Cell–Cell junctions in a monolayer are presumably weakened through a low dose of cytoB treatment or VE-cadherin antibody application, cell monolayer stiffness approaches that of single cells, and cell–substrate adhesion increases, suggesting the importance of Cell–Cell adhesions in signaling to the cell's mechanical machinery.

## MATERIALS AND METHODS

### Cell Culture

HUVECs were obtained from Lifeline Cell Technology (Walkersville, MD) and grown in tissue culture polystyrene flasks (Fisher Scientific, Pittsburgh, PA) at 37 °C, 5% CO<sub>2</sub>, and 55% humidity. HUVECs were cultured in VasculLife Basal Medium (Lifeline Cell Technology) supplemented with 2% fetal bovine serum (FBS), 10 mM L-glutamine, 0.2% EnGS, 5 ng/mL rhEGF, 1 μg/mL hydrocortisone hemisuccinate, 0.75 units/mL heparin sulfate (Lifeline Cell Technology), 10,000 units/mL penicillin, and 10,000 μg/mL streptomycin (Gibco, Carlsbad, CA) according to the manufacturer's specifications. HUVECs were split at 80–90% confluency, and passages 2–5 were used for experiments. Synchronization of cells was accomplished by (a) growing cells to confluency and (b) using low serum media (2%), according to Reinhart-King.<sup>57</sup> Glass coverslips (22 × 22 mm, No. 1.5, Fisher Scientific) were coated with 0.1 mg/mL fibronectin (Sigma, St. Louis, MO) for 2 h at room temperature. Cells were plated onto fibronectin-coated glass coverslips at high density ( $4 \times 10^5$  cells) and grown for approximately 48 h until monolayer formation. For single cell studies, HUVECs were plated at low density ( $8 \times 10^3$  cells), while for groups, HUVECs were plated at medium density ( $2 \times 10^4$  cells). Media was changed every 48–72 h. To weaken Cell–Cell junctions, two treatments were used: (a) HUVECs were treated with 2 μg/mL, 100 ng/mL, or 10 ng/mL cytochalasin B (Sigma) for 1 h at 37 °C, and (b) HUVECs were treated with 1:100 dilution (10 μg/mL) of anti-VE-cadherin (Sigma V1514) for 1 h at 37 °C just prior to experiments.

### Immunostaining

HUVECs were fixed in 2% paraformaldehyde (MP Biomedicals, Solon, OH) for 20 min, permeabilized in 1% TRITON-X 100 (VWR International, West Chester, PA) for 5 min, and blocked for non-specific binding in 2% bovine serum albumin (BSA; Sigma) for 1 h. For visualization of cellular borders, cells were incubated in primary antibody (rabbit polyclonal to β-catenin; Abcam ab2365, Cambridge, MA) at a 1:100 dilution (2 μg/mL) for 2 h. For visualization of focal adhesions, cells were incubated in primary antibody (anti-vinculin antibody, produced in mouse; Sigma V9131) at a 1:200 dilution (48 μg/mL) for 1 h. Non-specific binding was blocked again after primary antibody application in 2% BSA for 1 h. For β-catenin primary antibody, cells were incubated in secondary antibody (Rabbit Ig, Fluorescein-linked Whole Ab; GE Healthcare N1034, Piscataway, NJ) at a 1:20 dilution (105 μg/mL) for 1 h. For vinculin primary antibody, cells were incubated in secondary antibody (anti-mouse Alexa 488; Invitrogen A11001, Carlsbad, CA) at a 1:200 dilution (10 μg/mL) for 1 h. Primary and secondary antibodies were diluted in 2% BSA with phosphate buffered saline (PBS). For visualization of F-actin, cells were incubated in 0.1 μM Phalloidin-TRITC (Sigma) for 30 min. For nuclear staining, cells were treated with 2 μg/mL Hoechst stain (Invitrogen) for 5 min. All treatments were completed at room temperature. Cells were washed with PBS between each step.

## Atomic Force Microscopy

Young's moduli of live HUVEC monolayers were measured using an atomic force microscope (AFM; Agilent, Santa Clara, CA) with a silicon nitride cantilever (Novascan, Ames, IA) with a spherical glass SiO<sub>2</sub> probe of diameter 5 μM. The deflection sensitivity of the cantilever was measured using glass as a stiff surface. The cantilever spring constant was measured using Thermal K software (Molecular Imaging Corporation, San Diego, CA), where the cantilever was treated as a simple harmonic oscillator, according to the thermal fluctuation method.<sup>11,37</sup> The power spectrum of the AC signal was used to determine the mean-square amplitude of the cantilever, which was then used to solve for the spring constant. The manufacturer's nominal value for the cantilever spring constant (*k*) was 0.01 N/m, and the values obtained with Thermal K were within a factor of 2 (generally 0.006–0.008 N/m). Glass substrates with HUVECs attached were positioned under the AFM tip and typical force curves (Fig. 1A) were captured in different locations along the cells. All force curves and imaging were done at room temperature in FBS-free HUVEC media in an AFM liquid chamber.

The AFM procedure was begun by first scanning a region of interest (90 × 90 μM) using contact mode. Then, in the AFM Picoscan software, specific locations (25 per scan) were selected by hand, both at the periphery and cell body. The region of interest was scanned again and this time force vs. distance curves were taken at the chosen locations. Five to 20 images were obtained per sample, and 2–5 different samples were analyzed for each condition. The maximum size of the scan (90 μM × 90 μM) was large enough to capture most of one single cell per image and 3–6 cells within a monolayer per image. A force of approximately 2 nN was applied to the cells by the AFM cantilever, and this force was spread out over the large area of the 5 μM spherical probe attached to the cantilever, lessening the resulting applied traction. In performing AFM on living cells, AFM cantilevers containing spherical probes have an advantage over sharp tips, which can damage cells due to their tiny surface area (traction = force/area). AFM imaging and measurements were generally taken within 1 h.

In a custom-written Matlab (The MathWorks, Natick, MA) program, data were fit to the Hertz–Sneddon model<sup>66</sup> for a paraboloid indenter<sup>79</sup>:

$$F_{\text{paraboloid}} = \frac{4}{3} \left( \frac{E}{1 - \nu^2} \right) R^{1/2} \delta^{3/2},$$

where  $F_{\text{paraboloid}}$  is the force exerted by the paraboloid indenter,  $E$  is the Young's modulus of the cell,  $R$  is the radius of curvature of the indenter, and  $\delta$  is the distance of the indenter from the sample (Fig. 1B). Note that  $R$  for a sphere is equal to the radius of the sphere, and therefore  $R = 2.5 \mu\text{M}$  for the glass probe. The cells were assumed to be nearly incompressible<sup>46</sup> and therefore it was assumed that  $\nu = 0.45$  is the Poisson's ratio of the elastic halfspace. Note that the force is also equal to the cantilever spring constant ( $k$ ) times the change in position of the laser (as a measurement of the deflection of the cantilever). The Young's modulus was found for each force curve using the fitting algorithm. A maximum indentation of about 250 nm was chosen for fitting, since at small indentations the Young's modulus depends greatly on indentation depth,<sup>60</sup> while the Hertz–Sneddon model does not hold at large indentations. Two hundred fifty nanometers is sufficiently small compared to the height of the cell (several microns). The point of contact of the cantilever (Fig. 1A) with the sample was chosen to be the point at which the derivative of the force–distance curve became nonzero, or about 50 pN/nm. Thus, data were fit from the point of contact to the maximum indentation value. Average Young's modulus was computed by averaging all force curves for a given condition. Statistical tests were done using a Student's  $t$  test, where

$p < 0.05$  indicated statistical significance. All measurements reported in this article are in the format mean  $\pm$  standard error.

### Cell Spreading Combined with AFM

To determine the relationship between cell spreading and cell stiffness, HUVECs were trypsinized from tissue culture flasks, diluted with media, centrifuged, resuspended in FBS-free media, plated onto fibronectin-coated glass coverslips immediately, placed within the AFM liquid chamber, and allowed to attach to the substrate for 15–30 min before beginning AFM measurements. A low number of cells ( $8 \times 10^3$ ) were plated in order to ensure the presence of single cells on the surface of the coverslip. Cells that were relatively close to other cells were not analyzed, to avoid effects of Cell–Cell contact on the spreading process. The AFM tip was positioned over the cell. A minimal amount of cell attachment was necessary to ensure the cell did not move out from between the cantilever and the substrate. This level of attachment was determined through observation of the cell morphology in brightfield microscopy, when lamellipodia formation began. When this occurred, the AFM tip was lowered to the raised spherical central region of the cell (not the flattened periphery). AFM force measurements were taken every 30 s or 2 min during spreading without moving the cantilever horizontally in between measurements, and brightfield images were captured simultaneously every 30 s during spreading. Young's modulus was determined from force–distance curves as described in the previous section. To compute area, cells were traced by hand in ImageJ using a method previously described.<sup>68</sup> A sample size of  $N = 8$  spreading cells was used. A “morphology curve” was created using the spreading data, by plotting Young's modulus vs. area, with each data point representing the average area and Young's modulus of  $N = 8$  spreading cells at the same time points. Because the stiffnesses of spreading cells were averaged for each time point, and these data points included both periphery and cell body regions, the average stiffness of the periphery and cell body regions was plotted for each of single cells, groups, and monolayers.

### Phase Contrast, Confocal, and Total Internal Reflection Fluorescence Microscopy

Brightfield and phase contrast microscopy of HUVECs was completed at 37 °C, 5% CO<sub>2</sub> and 55% humidity using an inverted microscope (Olympus IX71, Center Valley, PA). Images were captured with a QImaging Retiga-SRV charge-coupled device (CCD) digital camera (QImaging Corporation, Surrey, British Columbia, Canada). Confocal microscopy was completed at room temperature on immunostained HUVECs using an inverted scanning disk confocal microscope (Olympus IX81). Images were captured with 0.3  $\mu$ m between planes on a Hamamatsu ORCA-ER CCD digital camera (Leeds Precision Instruments, Minneapolis, MN).

Total internal reflection fluorescence microscopy (TIRFM) was completed on samples (on  $n = 1.5$  glass coverslips) stained with vinculin antibody and FITC secondary antibody (as described above) at room temperature using an inverted microscope (Olympus IX81) using a 60 $\times$  oil immersion lens, as previously described.<sup>52</sup> Samples were illuminated with an ion laser of wavelength 488 nm (Melles Griot, Rochester, NY), and images were captured with a QImaging Rolera-MGi CCD digital camera (QImaging Corporation). The angle of laser incidence was adjusted once at the start of the experiment and was not adjusted between samples to ensure that the same plane was illuminated in each sample. In TIRFM, when the angle of incidence of light is greater than the critical angle for total internal reflection, an evanescent field is generated at the glass-sample interface. This evanescent field decays exponentially with distance normal to the interface, creating a thin layer of illumination ( $\leq 100$  nm<sup>3</sup>). TIRFM was chosen for imaging cell–substrate interactions over widefield fluorescence microscopy due to the thin layer of illumination which eliminates background fluorescence in TIRFM.

## Morphological Analysis

To aid with morphological analysis, HUVEC monolayers were fixed and immunostained for  $\beta$ -catenin in order to visualize cellular borders. For area analysis of single cells and cells within groups, individual HUVECs were traced by hand in ImageJ (National Institutes of Health, Bethesda, MD) using a method previously described.<sup>68</sup> For analysis of focal adhesion size and density we used the method as previously described.<sup>52</sup> Briefly, cells were stained for vinculin and TIRFM images were obtained. Images were made binary and the particle analyzer was used in ImageJ to measure vinculin punctuate sizes larger than  $0.5 \mu\text{m}^2$  and counts per area. Statistical tests were done using a Student's *t* test, where  $p < 0.05$  indicated statistical significance.

## RESULTS

### Cell Stiffness Measurements are Similar to Those Under Culture Conditions

Our AFM images and force curves on single cells, groups of cells, and monolayers were all performed at room temperature conditions. To evaluate the dependence of cell stiffness on temperature, CO<sub>2</sub>, and humidity, we measured the stiffness of single cells at both room temperature (23 °C) and culture conditions (37 °C with 5% CO<sub>2</sub> and 55% humidity) using an enclosed chamber. In our experimental set-up, performing AFM at room temperature vs. culture conditions does not make a difference (Fig. 1C). There is no statistical difference between the Young's moduli at the cell body ( $p = 0.34$ ;  $N = 326$  force curves from 30 cells at 23 °C and  $N = 181$  force curves from 14 cells at 37 °C) or periphery ( $p = 0.56$ ;  $N = 410$  force curves from 30 cells at 23 °C and  $N = 302$  force curves from 14 cells at 37 °C), according to a Student's *t* test. Distinction between cell body and periphery locations are later discussed in Fig. 3.

These results may differ from experiments where the cells are placed in room temperature medium, allowed to equilibrate to room temperature, and kept at room temperature for long periods of time, much longer than 1 h. In our experimental procedure, we removed cells directly from the incubator (conditioned at 37 °C and 5% CO<sub>2</sub>), washed them with PBS (warmed to 37 °C), and then added the media (also warmed to 37 °C) for AFM. Therefore, the cells began in a 37 °C environment. We imaged them and took force measurements for relatively short periods of time (under 1 h, as stated in our methods), though we would expect the media to cool moderately over the course of the experiment. However, we did not observe stiffening or softening of the cells over the course of AFM, further indicating that the temperature or CO<sub>2</sub> conditions did not affect our measurements during our experimental time window.

### Cell Area Depends on Degree of Cell–Cell Contact

HUVECs were plated at low, medium, or high density onto glass coverslips coated with fibronectin. At low density, single cells were observed. At medium density, cells were observed in groups of 3–13 cells where they formed isolated islands. At high density, cells formed confluent monolayers within 48 h.

We found that single cells are larger in area ( $2045 \pm 65 \mu\text{m}^2$ ;  $N = 167$  cells) than cells within a monolayer ( $1029 \pm 25 \mu\text{m}^2$ ;  $N = 192$ ,  $p < 0.001$ ), consistent with previous reports.<sup>51</sup> Cells in groups are larger ( $3030 \pm 73 \mu\text{m}^2$ ;  $N = 249$ ,  $p < 0.001$ ) than both single cells and cells in a monolayer (Fig. 2a). Phase contrast images of single cells (Fig. 2b), a group of 4 cells (Fig. 2c), and a monolayer of cells (Fig. 2d) show the differences in cell size as a function of degree of Cell–Cell contact.

## Single Cells are Stiffer Than Cells in a Monolayer

AFM was performed on HUVECs at varying degrees of Cell–Cell contact on fibronectin-coated glass substrates. AFM deflection images demonstrate the topography of a single HUVEC (Fig. 3a), group of three HUVECs (Fig. 3b), and monolayer of HUVECs (Fig. 3c). Each of these images indicates that the cell topography consists of both a raised portion, which likely contains the nucleus and other organelles and which we label the “cell body” (black arrows in Figs. 3a–3c), and also a more flattened region, which we label the “periphery” (white arrows in Figs. 3a–3c). We also compared the Young’s moduli of single cells at room temperature and at 37 °C with 5% CO<sub>2</sub> and 55% humidity and verified that under our experimental conditions AFM gave similar results.

For all degrees of Cell–Cell contact, the Young’s modulus of the periphery is larger than the Young’s modulus at the cell body location (Fig. 3d). We found that the Young’s modulus of single cells is larger than that of monolayers, both at the cell body ( $E = 854 \pm 39$  Pa,  $N = 195$  for single cells and  $E = 757 \pm 16$  Pa,  $N = 246$  for monolayers,  $p = 0.013$ ) and periphery locations ( $E = 1558 \pm 46$  Pa,  $N = 284$  for single cells and  $E = 1042 \pm 14$  Pa,  $N = 457$  for monolayers,  $p < 0.001$ ) (Fig. 3d). At the cell body ( $E = 886 \pm 72$  Pa,  $N = 44$  for groups of 3 cells;  $E = 880 \pm 76$ ,  $N = 67$  for 4–5 cells; and  $E = 786 \pm 130$ ,  $N = 16$  for groups of 6–13 cells), the Young’s modulus of groups of 3–5 and groups of 6–13 cells is not different from that of single cells ( $p > 0.600$ ), while at the periphery ( $E = 1899 \pm 60$  Pa,  $N = 100$  for groups of 3 cells;  $E = 1742 \pm 70$ ,  $N = 98$  for 4–5 cells; and  $E = 1738 \pm 106$ ,  $N = 46$  for groups of 6–13 cells) the Young’s modulus is larger than both single cells ( $p < 0.001$ ,  $p = 0.037$ ,  $p = 0.139$ , respectively with increasing group size) and monolayers ( $p < 0.001$  for all groups) (Fig. 3d).

Further, the distributions of Young’s moduli for single cells (Fig. 3e), groups (Fig. 3f), and monolayers (Fig. 3g) indicate the large variation in stiffness among cells, even when looking at the same region (cell body or periphery). These distributions show that for single cells and groups, the distributions are fairly wide (Figs. 3e, 3f), while for monolayers, the distributions are much tighter (Fig. 3g). Thus, monolayers are more homogeneous in terms of stiffness than both groups and single cells.

## Cell Stiffness Increases During Spreading

One approach to determine the relationship between cell morphology and stiffness is to measure the stiffness and area of a single cell simultaneously as it spreads (Fig. 4). We performed this experiment by obtaining brightfield timelapse images while taking AFM force curves on a single spreading cell following trypsinization. Note that we did not scan the cell with AFM, but rather the cantilever remained stationary (in the horizontal plane) as the cell spread. Following the typical cell spreading process,<sup>58</sup> the HUVECs began as spheres upon plating, presumably formed initial adhesions to the substrate upon lamellipodium formation (Fig. 4d,  $T = 0$ ), and spread fairly isotropically onto the substrate over the course of 1 h (Figs. 4d, 4e). HUVECs flattened as they spread, as it was necessary to bring the sample closer to the AFM cantilever during spreading in order to avoid flat-lining the force–distance curves.

We found that for all cells probed ( $N = 8$  cells), the Young’s modulus of the cell increased as spreading area increased (Fig. 4). This behavior was independent of how often the cell was probed with the AFM cantilever (every 30 s in Figs. 4a and 4b and every 2 min in Fig. 4c). The Young’s modulus at the initial timepoint ( $E \sim 400$  Pa) indicates a lower bound of cell stiffness, where the cell is (visibly) slightly attached to the substrate as determined by brightfield microscopy, but still is round in morphology. The Young’s modulus at this point is very similar to that when cells have been treated with cytoB to disrupt F-actin (gray

outlined dots at time = 0 in Fig. 4). See text below and Figs. 6a–d for more discussion on the effects of cytoB treatment.

### Cell Stiffness and Spreading Area Correlate for Single Cells and Groups

Using the data obtained from performing AFM on spreading cells, we also plotted Young's modulus vs. area, with each data point indicating the average Young's modulus and area of  $N = 8$  cells (Fig. 5) at the same time point. We call this the "morphology curve." The white outlined circles in Fig. 5 therefore represent the measured Young's modulus of a cell, given its area. We found that the (area, stiffness) of single cells and groups both lie on this curve, while monolayers are stiffer than expected (Fig. 5). Furthermore, monolayers treated with 2  $\mu\text{g}/\text{mL}$  cytoB do lie on the measured morphology curve, while monolayers treated with VE-cadherin antibody and 10 ng/mL cytoB lie above it.

### Cell Stiffness is Dependent on Concentration of Cytochalasin B

Cell–Cell adhesions in a monolayer can be broken or weakened via several methods. In the extreme, they can be completely disrupted by interfering with the F-actin network, which is critical for maintaining Cell–Cell junctions and tensional homeostasis within the cells. We used the cytoB treatment to cap actin filaments, preventing further polymerization and leading to net depolymerization of the filaments. It has previously been reported that cells soften when treated with drugs of the cytochalasin family.<sup>62,75</sup>

We treated HUVECs with decreasing concentrations of cytoB to vary the amount of F-actin disruption. The mechanical response of the monolayer depended on the concentration of drug applied (Fig. 6a). With the highest concentration of cytoB (2  $\mu\text{g}/\text{mL}$ ; "high"), the average Young's modulus is smaller than control cells, both at the cell body ( $E = 454 \pm 27$  Pa,  $N = 70$ ,  $p < 0.001$ ) and periphery locations ( $E = 583 \pm 29$  Pa,  $N = 22$ ,  $p < 0.001$ ). With this treatment, the monolayer is completely disrupted, as evidenced in the AFM deflection image (Fig. 6b), where the HUVECs have undergone significant rounding due to the high degree of actin depolymerization. With a smaller concentration of cytoB (100 ng/mL; "intermediate"), the average Young's modulus is smaller than control cells at the cell body ( $E = 623 \pm 26$ ,  $N = 110$ ,  $p < 0.001$ ), but it is not different from control cells at the periphery ( $E = 986 \pm 30$ ,  $N = 198$ ,  $p = 0.051$ ). AFM deflection images indicate that with this amount of F-actin disruption, some Cell–Cell adhesions have remained intact; however, there are also large gaps in the monolayer where the cells have retracted and Cell–Cell adhesions are disrupted (Fig. 6c). Finally, with the least harsh treatment of cytoB (10 ng/mL; "low"), the Young's modulus is surprisingly larger than control cells, both at the cell body ( $E = 1157 \pm 46$ ,  $N = 116$ ,  $p < 0.001$ ) and periphery ( $E = 1524 \pm 43$ ,  $N = 176$ ,  $p = 0.004$ ). With this treatment, the cell monolayer is still mostly visibly intact, with some disruption indicated by the presence of tether-like structures between adjacent cells (Fig. 6d; white arrowheads). These tether-like structures are present at many Cell–Cell adhesion sites. There is no statistical difference in area of the cells, compared with cells in control monolayers. The Young's modulus of cell monolayers treated with low cytoB is not different from control single cells at the periphery region, while it is different at the cell body region.

### Monolayers Stiffen When Junctions are Destabilized with VE-Cadherin Antibody

A second approach to destabilizing Cell–Cell adhesions in HUVEC monolayers is by applying a VE-cadherin antibody. We found that in HUVEC monolayers, treatment with a VE-cadherin antibody results in an increase in Young's modulus, both at the cell body ( $E = 908 \pm 21$ ,  $N = 241$ ,  $p < 0.001$ ) and periphery ( $E = 1214 \pm 14$ ,  $N = 583$ ,  $p < 0.001$ ) (Fig. 6e). Meanwhile, there is no difference in cell area, compared with control monolayers.

To determine the baseline effect of the VE-cadherin antibody when no Cell–Cell adhesions are present, we performed the same experiment on single cells. Interestingly, single cells treated with a VE-cadherin antibody are softer than control cells, both at the cell body ( $E = 623 \pm 28$ ,  $N = 84$ ,  $p < 0.001$ ) and periphery ( $1387 \pm 61$ ,  $N = 160$ ,  $p = 0.025$ ). Further, VE-cadherin antibody-treated cells follow the trend that single cells are stiffer than cells within a monolayer. AFM deflection images of single cells and monolayers treated with VE-cadherin antibody do not look different from images of control cells (Figs. 6f, 6g).

### Actin Cytoskeleton Architecture Depends on Degree of Cell–Cell Contact

We used confocal imaging of phalloidin–actin-stained samples to evaluate the architecture of the F-actin network as a function of degree of Cell–Cell contact. We found that control single cells and groups have well-developed stress fibers arranged in parallel throughout the entire length and width of the cell, and most of these stress fibers within a given cell are oriented locally in the same direction (Figs. 7a, 7b). Cells in monolayer also have well-developed stress fibers, yet they are oriented mostly around the cell borders, with only some extending along the length of the cell (Fig. 7c). Cells treated with  $2 \mu\text{g}/\text{mL}$  cytoB show complete disruption of F-actin, as expected (Fig. 7d). Cells treated with  $100 \text{ ng}/\text{mL}$  show significant monolayer disruption, with several F-actin filaments or bundles tethering to neighboring cells (Fig. 7e; white arrowheads). Meanwhile, in cells treated with a very low dose of cytoB ( $10 \text{ ng}/\text{mL}$ ), we do not observe differences in F-actin arrangement as compared to control monolayers (Fig. 7f). Further, the F-actin structure of both single cells and monolayers treated with VE-cadherin antibody do not show differences as compared with the controls (Figs. 7g, 7h).

### Focal Adhesion Size and Density Depend on Degree of Cell–Cell Contact

To determine whether differences in cell stiffness could be partially explained by focal adhesion (FA) assembly,<sup>30,52</sup> we immunostained for vinculin, performed total internal reflection microscopy (TIRFM) on the samples (Figs. 7i, 7j), and measured the size and density of FAs as a function of degree of Cell–Cell contact. We found that FAs in monolayers are the same size as in single cells ( $\sim 1.4 \mu\text{m}^2$ ,  $p = 0.900$ ; Fig. 7k), but there are less FAs per area in monolayers ( $p < 0.001$ ; Fig. 7l). FAs in groups are larger than in single cells ( $\sim 1.6 \mu\text{m}^2$ ,  $p < 0.001$ ) but are present at the same density as in single cells ( $p = 0.501$ ; Fig. 7l). FAs in single cells treated with VE-cadherin antibody are not different in size from FAs in control single cells ( $p = 0.289$ ; Fig. 7k), but, interestingly, they are more densely arranged ( $p < 0.001$ ; Fig. 7l). Finally, FAs in monolayers treated with VE-cadherin antibody or a low dose of cytoB are larger than FAs in control monolayers ( $p < 0.001$ ; Fig. 7k), and FAs in both treatments are more dense ( $p < 0.001$ ; Fig. 7l). FAs of cell monolayers treated with intermediate ( $100 \text{ ng}/\text{mL}$ ) and high ( $2 \mu\text{g}/\text{mL}$ ) doses of cytoB were significantly dissolved and thus we did not measure their size or density.

## DISCUSSION

Our data suggest that cell area correlates roughly with cell stiffness. However, in groups or in monolayers, cells have several neighbors, and Cell–Cell interactions likely play a role in determining cell stiffness. It was our goal to determine whether cell mechanics is necessarily governed by spreading area or whether Cell–Cell interactions play a significant role in determining the mechanical properties of cells within a monolayer.

Our rationale for evaluating the stiffness of groups of cells was to have a system in which the size of the cells was similar to that of single cells, yet Cell–Cell adhesions were also present. However, we observed that cells in groups of cells are actually larger (by a factor of  $\sim 1.5$ ), and also stiffer, than single cells (Figs. 2, 3). One possibility is that the cells, after

coming in contact with another cell or group of cells, are extending toward the free periphery, away from the group, to facilitate migration. This is reminiscent of the leading edge of an epithelial cell sheet, where microtubule plus ends are very dynamic near free non-contacted cell edges and suppressed at Cell–Cell contacts; further, the continuous polymerization and retrograde flow of actin which is necessary for cell motility is inhibited at Cell–Cell contacts.<sup>78</sup> Some degree of Cell–Cell adhesion has already formed at this point, and the cell's area may increase because it is attempting to move away from the group, as in EC sheet migration.<sup>74</sup> If this is true, it is possible that the larger cell contains an actin cytoskeleton-plasma membrane cortex which is under more tension than in smaller, single cells. Experimentally, we measure larger FAs in groups than in single cells (Fig. 7k), and because traction forces and FA area are correlated<sup>4</sup> and also F-actin tension and cell stiffness are correlated,<sup>77</sup> we believe that stress fiber tension may be increased in groups, even though we do not observe differences in F-actin structure. This is in agreement with the reports of Califano and Reinhart-King<sup>15</sup> where cell traction forces increase when two cells come in contact. Further, cells in a monolayer are tightly packed and smaller (Fig. 2), with less FAs per area (Fig. 7l) and stress fibers oriented mainly around the cell borders (Fig. 7c), possibly leading to decreased F-actin tension and decreased cell stiffness compared with single cells and groups. The decreased FA density and rearrangement of F-actin in monolayers suggests that the monolayer integrity is maintained more through Cell–Cell contacts than through cell–substrate contacts, while single cells must rely solely on cell–substrate adhesion for support.

Previously, it has been shown by Nelson *et al.*<sup>51</sup> that cell area and FA area both decrease with increasing cell density through activation of RhoA, which is in contrast to the increased cell area and FA size in our groups. However, in Nelson *et al.*, when spreading area is confined using a micropatterned substrate, FA size is larger for two cells in contact, as compared with a single cell, which is in agreement with our results for groups. It could be possible that in our experiments, our cells had more free space around them during group formation, allowing for outward extension, while in Nelson *et al.* there was an increased cell density which restricted cell size. It would be interesting to investigate the effects of Cell–Cell contact length on FA size; using a micropatterned substrate, this could be achieved by increasing or decreasing the Cell–Cell contact region in Nelson *et al.*'s bowtie configuration.

To corroborate the notion that cell morphology affects cell stiffness, we simultaneously measured the stiffness and area of a spreading cell using AFM combined with brightfield timelapse images. This experiment allowed us to observe changes in cell area without the presence of neighboring cells or Cell–Cell adhesions. Our measurements began when the cells were approximately 30–40% of their final spreading area. Our results show that HUVECs increase in stiffness as they spread (Fig. 4), which might be expected since they transform from round spheres with a layer of cortical actin, to spread-out objects adhering to the substrate and containing a stiff network of cross-linked actin filaments and cortical actin under tension.<sup>6</sup> The value which the final Young's modulus approaches provides a rough indication of whether the cell body (compare with gray large dashed line in Fig. 4) or periphery (compare with gray small dashed line in Fig. 4) has been probed. For example, in Figs. 4a and 4b the periphery is likely being probed, while in Fig. 4c it is likely the cell body. We believe that the force exerted by the AFM cantilever had minimal effect on cell spreading, as we did not observe differences in spreading when we increased the time interval (30 s to 2 min) between “pokes” with the AFM cantilever. Further, HUVEC spreading in the presence of the AFM cantilever was similar to spreading in its absence, suggesting that the AFM tip itself had minimal impact on cell spreading. Further, using an AFM tip which contained a 5  $\mu$ M bead was much gentler than using a sharp 10 nm-sized tip, which resulted in irregular spreading behavior.

Further, our results are consistent with the measurements that cell traction forces increase during spreading.<sup>58</sup> Interestingly, another previous study by Gauthier *et al.*<sup>29</sup> showed that membrane tension decreases during cell spreading, as measured by optical tweezers. However, this is not necessarily contradictory to our results. Because the thickness of the cell membrane is only on the order of 3–4 nm,<sup>56</sup> and we are probing approximately 250 nm into the cell, we are likely measuring the stiffness of the cortical actin rather than the cell membrane. Although the cell membrane and cortex are physically linked, the cortex likely provides more resistance to the AFM cantilever than the cell membrane itself, resulting in a stiffer measurement. Therefore, if it is true that the cell membrane softens during spreading, we would not be able to detect it.

The “morphology” curve represented by Fig. 5 may be interpreted as the measured stiffness of a cell, given its area, and we can use it to roughly predict a cell’s stiffness knowing its area. Interestingly, when we plot the average (area, stiffness) of single cells and groups (data from Figs. 2, 3), the points lie on the morphology curve. However, the average (area, stiffness) of monolayers (data from Figs. 2, 3) lies above the curve, indicating that its stiffness is higher than we would expect based on its area. Further, when we depolymerize actin filaments using a high dose of cytoB, the monolayer is completely disrupted, and the (area, stiffness) of the cells returns to lie on the morphology curve. If we weaken junctions (e.g., through treatment with VE-cadherin antibody or a low dose of cytoB), the monolayer stiffness increases to further from the morphology curve. Therefore, it seems possible that Cell–Cell contacts influence cell mechanical properties, but the form of this influence is currently unknown.

To further investigate the effects of Cell–Cell junction integrity on cell stiffness, we first used a titration of cytoB treatment to destabilize the Cell–Cell junctions to varying degrees. At the lowest dose of cytoB, the HUVEC monolayers show small disruption in Cell–Cell adhesions, indicated by tether-like structures at cell junctions in the AFM deflection image (white arrowheads in Fig. 6d) while the F-actin does not appear to have changed (Fig. 7f). Interestingly, the monolayer remains visibly intact, except for the tether-like structures, and there is an increase in cell stiffness (Fig. 6a). This could in part be explained by the increased FA size and density with low cytoB treatment (Fig. 7l), which may generate increased tension within the cells, even though we do not see differences in F-actin architecture. It could be possible that the low dose of cytoB is only affecting the cortical actin along the cell membrane, which might affect the overall tension balance in the cell. This may lead the stress fibers to take up some of the tension, resulting in increased cell–substrate adhesion and decreased Cell–Cell adhesion. Thus, with low cytoB treatment, it seems that we disrupt the Cell–Cell junctions minimally (according to AFM images) without completely breaking the cells apart and the stiffness of cells within the monolayer approaches that of single cells.

Our second approach to destabilize cell junctions was to apply a VE-cadherin antibody to the HUVEC monolayers. VE-cadherin is a homophilic protein which localizes to cellular junctions and binds to actin, leading to maintenance of tension between cells.<sup>2,22</sup> Further, VE-cadherin engagement has been demonstrated to activate RhoA,<sup>51</sup> which would result in an increase in cell tension and stiffness. Treatment of EC monolayers with a VE-cadherin antibody decreases Cell–Cell adhesivity and increases monolayer permeability.<sup>18,32,35</sup> Thus, the treatment weakens Cell–Cell junctions without completely breaking them.<sup>35</sup> We expected that molecular engagement of homophilic VE-cadherin might be similar to the presence of leukocytes attempting to transmigrate at cell borders and therefore cause rearrangement of VE-cadherin away from the junction, an effect which has previously been validated.<sup>35</sup> We thought that the resulting effect would be similar to cytoB treatment, where the monolayers approach the stiffness of single cells. However, VE-cadherin is one of many

proteins localized at Cell–Cell junctions, and how the antibody treatment affects the localization or bond strength of other homophilic junctional proteins remains unknown.

Despite the potential involvement of other junctional proteins, our results agree with the above hypothesis—HUVEC monolayers stiffen with VE-cadherin antibody treatment (Fig. 6e). Though we do not observe changes in F-actin structure (Fig. 7h), the increased size and density of FAs (Figs. 7k, 7l) may cause the F-actin tension of cells within the monolayer to increase and approach that of single cells. It has been shown that development of cadherin adhesions causes an increase in integrin expression,<sup>81</sup> as well as recruitment of vinculin to Cell–Cell adhesions, leading to a reduction in vinculin at FAs,<sup>45</sup> so the opposite process may also be true, according to our results. Also in agreement with our data, de Rooij *et al.*<sup>21</sup> showed that epithelial cell scattering is induced by increased tension on Cell–Cell junctions (e.g., on stiffer surfaces or on extracellular matrices which promote larger FAs), suggesting that the F-actin cytoskeleton mediates a cross-talk between cadherins in Cell–Cell junctions and integrins at the cell–substrate interface.

Further, we probed the stiffness of single cells treated with a VE-cadherin antibody in order to evaluate whether the antibody itself results in any changes in cell stiffness, possibly due to signaling events that are not associated with weakened cellular junctions. Neither the higher density of FAs (Fig. 7l) nor the F-actin arrangement (Fig. 7g) can account for the softening of the cells. We would expect the higher density of FAs to result in an overall increase in cell tension; however, the softening of the cells does not support this idea. While we do not know the specific reason for this softening, it seems obvious that VE-cadherin antibody treatment affects single cells differently than cells within a monolayer, further suggesting the importance of Cell–Cell adhesions in determining cell stiffness. Localization of VE-cadherin in single cells and monolayers is very different, and engagement of VE-cadherin in these two situations likely results in differences in activation of signaling pathways. For example, in monolayers, VE-cadherin localizes to Cell–Cell junctions and is physically linked to the actin cytoskeleton; this localization occurs when the cell meets a neighboring cell.<sup>51</sup> Thus, in single cells, engagement of VE-cadherin may result in biophysical changes which are not accounted for in our experiments and which cause softening of the cells.

In all experiments we observe that the cell periphery is statistically stiffer than the cell body. Previous studies have reported measurements that are both consistent with<sup>61</sup> and contradictory to<sup>64</sup> our finding. Possible reasons for disagreement in literature over whether the cell body or periphery is stiffer include the following: (a) differences in the amount of force applied to the cells and the timescale over which those forces are exerted, both of which influence the measured mechanical properties of a viscoelastic material such as a cell; (b) differences in the maximum indentation fitted using the Hertz–Sneddon model, since very large indentations likely cause the stiff glass substrate to influence elastic measurements; and (c) differences in positioning of the AFM cantilever over the cell body, since the nucleus is the stiffest organelle in the cell (for review see Dahl *et al.*<sup>19</sup>) and is located in what we call the “cell body” region. Our force curves are taken by applying a small force, about 2 nN, over the course of 1 s. To eliminate the effects of the glass substrate, we fit our force curves to only the first 250 nm of indentation, which is small compared to the height of the cell, even at the periphery, which is about 600–800 nm in thickness, as measured by AFM topographic images. Further, because we are simultaneously obtaining AFM topographic images and force curves, we were able to choose to place the 25 force curve buffers at any region on the cell. While we did not know the exact position of the nucleus, our measurements show that consistently, the cell body is softer than the periphery, suggesting that we are not probing deep enough into the cell to “feel” the nuclear stiffness. Probing with deeper indentations into the cell could result in

measurement of the stiffness of other structures within the cell, such as intermediate filaments, which have been shown to be important mechanotransducers within the cell.<sup>33,76</sup> However, it has been shown that F-actin is the main contributor to cell stiffness,<sup>28</sup> and that cell types with more pronounced F-actin networks (e.g., lymphocytes) are stiffer than cell types with less F-actin (e.g., Jurkat cells<sup>13</sup>). In previous reports, increased indentation depths led to two distinct slopes in the AFM force–distance curves,<sup>40,53</sup> corresponding to measurement of the stiffness of two distinct mechanical regions within the cell. Much further experimentation and analysis are necessary to determine exactly which cellular structures and their interactions contribute to cellular stiffness. It would also be useful to identify whether the applied forces activate biochemical signaling pathways within the cell, perhaps through mechanosensitive transmembrane proteins such as syndecan-4.<sup>5</sup>

To summarize our observations regarding cell spreading, single cell to monolayer transition, and the effects of Cell–Cell adhesions in a monolayer, we created a schematic (Fig. 8). In Fig. 8a, the organization of cortical actin and stress fibers are based on the experimental observations of spreading cells, as previously described.<sup>6,58</sup> According to these reports, a cell begins as a round sphere containing a layer of cortical actin. As it touches down onto the substrate and begins to form adhesions, actin polymerization initializes at the basal surface, with a layer of cortical actin remaining at the apical surface. At this point, there is probably still a low level of tension in the cell due to the immaturity of the F-actin filaments. The force of actin polymerization extends the periphery of the cell outward, and eventually mature stress fibers form, likely leading to an increase in internal tension within the cell. The final spread cell probably consists of a dense layer of highly cross-linked stress fibers stretched along the basal surface of the cell and an apical layer of cortical actin, which presumably also has undergone an increase in tension. We believe that this potential increase in tension of the F-actin architecture contributes to the overall increase in cell stiffness and is likely caused by myosin II, a motor protein known to cross-link actin filaments and subsequently pull on them. Previously, it has been shown that inhibition of myosin II via blebbistatin treatment leads to a decrease in cell stiffness and also causes cell retraction.<sup>48</sup> This experimental observation agrees with our proposed model (Fig. 8a); if we remove myosin II, the stress fiber cross-links, the cell loses tension, causing relaxation of the actin cytoskeleton and a decrease in cell stiffness. Ultimately, in the cell spreading model, this would revert the cell to an earlier, softer, spreading state.

In Fig. 8b, the transition from single cell to group to monolayer is summarized, according to our observations. Beginning in solitude, the spread cell contains a dense network of stress fibers, oriented locally in parallel groups. Eventually, more cells join the first cell and form what we refer to as a group, shown here as an island of four cells, all with Cell–Cell adhesions at the interior. While the F-actin architecture does not look significantly different from that of the single cell, we propose that the cells are extending outward at the periphery through actin polymerization, as evidenced by the increased size of both the cells and their FAs, yet they are still visibly connected to each other through Cell–Cell adhesions. The force of extension may generate more tension within the cells and thus an increase in cell stiffness. Then, as more and more cells enter the group, they begin packing and eventually form a monolayer. Note that in our schematic cartoon, the monolayer continues outward infinitely in all directions; pictured are cells at the interior. For reference, the compressive forces due to cell packing in the epithelial layer during morphogenesis have been measured to be quite sizeable.<sup>27,36</sup> The stress fibers are arranged mainly around the periphery of the cell, suggesting that rearrangement has occurred due to the cell packing forces, resulting in softer cells. In a monolayer, there are less FAs per area, indicating that cell–substrate adhesion has decreased, but Cell–Cell adhesion has probably increased due to the formation of adherens junctions. The actin is linked to the cellular junctions through VE-cadherin, and

the VE-cadherin molecules on neighboring cells link to each other, creating a physical link between cells through which force can be transferred.

In Fig. 8c, we propose a sketch which summarizes our observation on the effects of applying a VE-cadherin antibody or a low dose of cytoB, treatments which we or others have suggested to weaken Cell–Cell adhesions. Initially, the cell monolayer contains some degree of Cell–Cell and cell–substrate adhesions. Then, upon treatment to weaken the Cell–Cell adhesions, the cell–substrate adhesions become stronger as evidenced experimentally by larger and more area-dense FAs. Though we do not observe differences in F-actin architecture between the two monolayer states, the increased FAs suggest an increase in F-actin tension, resulting in a stiffer monolayer. Mechanically, the cell may seek to achieve a balance between Cell–Cell adhesion through cadherin activation and cell–substrate adhesion through integrin activation, and as one adhesion is decreased, the other increases.<sup>44,63</sup>

Previously, it has been shown that matrix properties such as substrate stiffness and extracellular matrix (ECM) coating affect cell–substrate adhesion, spreading area, and cell stiffness. In particular, cells have been found to spread less on softer surfaces and those with a low density of ECM protein at the surface, while cells spread more on stiffer surfaces and those with a higher density of ECM protein.<sup>14,23,38,58,68,80</sup> Further, cell stiffness increases as substrate stiffness increases<sup>12,31,67</sup> and as ECM density increases.<sup>7</sup> Together, these observations agree with our results, where increased spreading area correlates with increased cell stiffness. However, many of these experiments have been completed on single cells, and the role of substrate stiffness and ECM density in influencing Cell–Cell adhesion strength is only beginning to be understood. For example, Califano and Reinhart-King<sup>14</sup> have shown that softer surfaces with high ECM density promote formation and maintenance of Cell–Cell adhesions in EC networks, while EC networks do not form on stiffer surfaces with low ECM density. Further support of this idea is the work of de Rooj *et al.*<sup>21</sup> where epithelial Cell–Cell connections are disrupted through scattering on stiff surfaces and on those with high ECM density. These results suggest that both mechanical and chemical cues are incorporated as cells balance Cell–Cell and cell–substrate interactions. Further experiments where matrix mechanical and chemical properties are manipulated are definitely necessary to build upon our understanding of the relationships between cell morphology, cell stiffness, and Cell–Cell and cell–substrate adhesion.

In summary, cells within a monolayer are spatially confined due to the presence of neighbors and also have close adhesions with these neighbors at the junctions. In varying the degree of Cell–Cell contact in HUVECs (single cells, groups, and monolayers), we observe that increased cell stiffness roughly correlates with an increase in cell area. Further, we see that HUVECs stiffen as they spread onto a glass substrate. When we treat the cells with a low dose of cytoB or VE-cadherin antibody, treatments which presumably weaken Cell–Cell adhesions, we measure that cell–substrate adhesion increases, and the stiffness of cells within the monolayer approaches that of single cells. Our results together suggest that while morphology can roughly be used to predict cell stiffness, Cell–Cell interactions may play an important role in determining the mechanical properties of cells through maintenance of the balance between Cell–Cell and cell–substrate interactions. This biophysical balance may be disrupted in biological processes such as wound healing, angiogenesis, cancer cell metastasis, and immune cell transmigration.

## Acknowledgments

This work was completed under an NSF Graduate Research Fellowship to KMS, NIH NRSA fellowship to KMS (NINDS Award Number F31NS068028) and NSF Award CMMI-0643783 to HAE. The content is solely the responsibility of the authors and does not necessarily represent the official views of the National Institute of Neurological Disorders and Stroke or the National Institutes of Health.

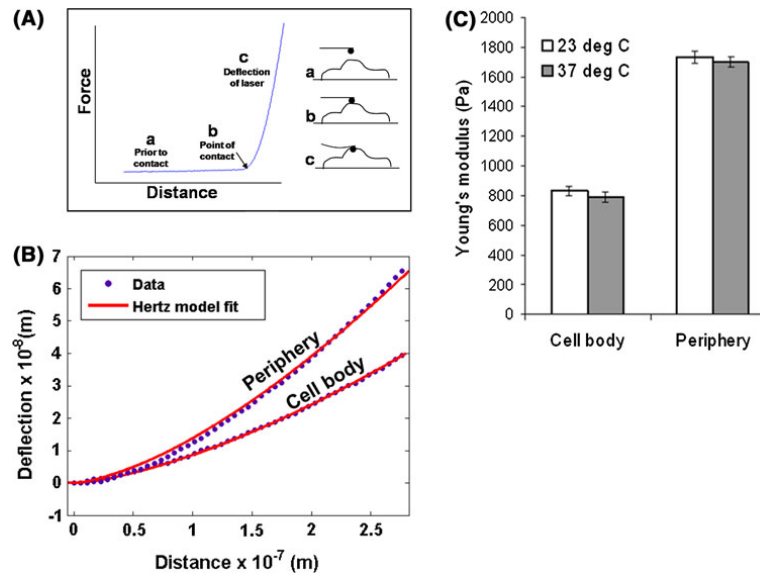
## REFERENCES

1. Adams CL, Nelson WJ. Cytomechanics of cadherin-mediated Cell–Cell adhesion. *Curr. Opin. Cell Biol* 1998;10:572–577. [PubMed: 9818166]
2. Angst BD, Marozzi C, Magee AI. The cadherin superfamily: diversity in form and function. *J. Cell Sci* 2001;114:629–641. [PubMed: 11171368]
3. Axelrod D. Total internal reflection fluorescence microscopy in cell biology. *Traffic* 2001;2:764–774. [PubMed: 11733042]
4. Balaban NQ, Schwarz US, Riveline D, Goichberg P, Tzur G, et al. Force and focal adhesion assembly: a close relationship studied using elastic micropatterned substrates. *Nat. Cell Biol* 2001;3:466–472. [PubMed: 11331874]
5. Bellin RM, Kubicek JD, Frigault MJ, Kamien AJ, Steward RL, et al. Defining the role of syndecan-4 in mechanotransduction using surface-modification approaches. *Proc. Natl Acad. Sci. USA* 2009;106:22102–22107. [PubMed: 20080785]
6. Bereiterhahn J, Luck M, Miebach T, Stelzer HK, Voth M. Spreading of trypsinized cells—cytoskeletal dynamics and energy-requirements. *J. Cell Sci* 1990;96:171–188. [PubMed: 2373741]
7. Bhadriraju K, Hansen LK. Extracellular matrix- and cytoskeleton-dependent changes in cell shape and stiffness. *Exp. Cell Res* 2002;278:92–100. [PubMed: 12126961]
8. Blacher J, Asmar R, Djane S, London GM, Safar ME. Aortic pulse wave velocity as a marker of cardiovascular risk in hypertensive patients. *Hypertension* 1999;33:1111–1117. [PubMed: 10334796]
9. Blaschuk OW, Devemy E. Cadherins as novel targets for anti-cancer therapy. *Eur. J. Pharmacol* 2009;625:195–198. [PubMed: 19836380]
10. Boutouyrie P, Tropeano AI, Asmar R, Gautier I, Benetos A, et al. Aortic stiffness is an independent predictor of primary coronary events in hypertensive patients—a longitudinal study. *Hypertension* 2002;39:10–15. [PubMed: 11799071]
11. Butt HJ, Jaschke M. Calculation of thermal noise in atomic-force microscopy. *Nanotechnology* 1995;6:1–7.
12. Byfield FJ, Reen RK, Shentu TP, Levitan I, Gooch KJ. Endothelial actin and cell stiffness is modulated by substrate stiffness in 2D and 3D. *J. Biomech* 2009;42:1114–1119. [PubMed: 19356760]
13. Cai XF, Xing XB, Cai JY, Chen Q, Wu SX, Huang FC. Connection between biomechanics and cytoskeleton structure of lymphocyte and Jurkat cells: an AFM study. *Micron* 2010;41:257–262. [PubMed: 20060729]
14. Califano JP, Reinhart-King CA. A balance of substrate mechanics and matrix chemistry regulates endothelial cell network assembly. *Cel. Mol. Bioeng* 2008;1:122–132.
15. Califano JP, Reinhart-King CA. Substrate stiffness and cell area predict cellular traction stresses in single cells and cells in contact. *Cel. Mol. Bioeng* 2010;3:68–75.
16. Chen CS, Mrksich M, Huang S, Whitesides GM, Ingber DE. Geometric control of cell life and death. *Science* 1997;276:1425–1428. [PubMed: 9162012]
17. Chouinard JA, Grenier G, Khalil A, Vermette P. Oxidized-LDL induce morphological changes and increase stiffness of endothelial cells. *Exp. Cell Res* 2008;314:3007–3016. [PubMed: 18692495]
18. Corada M, Mariotti M, Thurston G, Smith K, Kunkel R, et al. Vascular endothelial-cadherin is an important determinant of microvascular integrity in vivo. *Proc. Natl Acad. Sci. USA* 1999;96:9815–9820. [PubMed: 10449777]
19. Dahl KN, Ribeiro AJS, Lammerding J. Nuclear shape, mechanics, and mechanotransduction. *Circ. Res* 2008;102:1307–1318. [PubMed: 18535268]
20. Davies PF, Barbee KA, Volin MV, Robotewskyj A, Chen J, et al. Spatial relationships in early signaling events of flow-mediated endothelial mechanotransduction. *Annu. Rev. Physiol* 1997;59:527–549. [PubMed: 9074776]
21. de Rooij J, Kerstens A, Danuser G, Schwartz MA, Waterman-Storer CM. Integrin-dependent actomyosin contraction regulates epithelial cell scattering. *J. Cell Biol* 2005;171:153–164. [PubMed: 16216928]

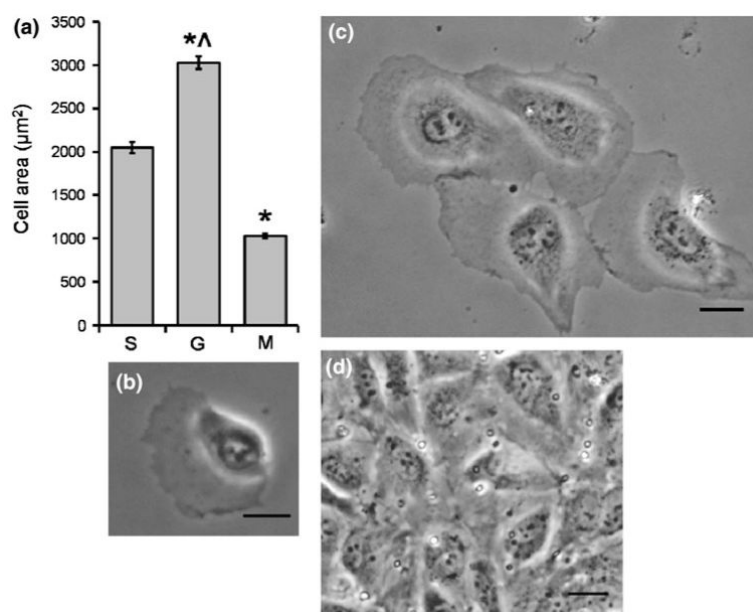
22. Dejana E. Endothelial Cell–Cell junctions: happy together. *Nat. Rev. Mol. Cell Biol* 2004;5:261–270. [PubMed: 15071551]
23. Engler A, Bacakova L, Newman C, Hategan A, Griffin M, Discher D. Substrate compliance versus ligand density in cell on gel responses. *Biophys. J* 2004;86:617–628. [PubMed: 14695306]
24. Etienne-Manneville S, Hall A. Rho GTPases in cell biology. *Nature* 2002;420:629–635. [PubMed: 12478284]
25. Fagotto F, Gumbiner BM. Cell contact-dependent signaling. *Dev. Biol* 1996;180:445–454. [PubMed: 8954717]
26. Farhadifar R, Roper JC, Algouy B, Eaton S, Julicher F. The influence of cell mechanics, Cell–Cell interactions, and proliferation on epithelial packing. *Curr. Biol* 2007;17:2095–2104. [PubMed: 18082406]
27. Foty RA, Pflieger CM, Forgacs G, Steinberg MS. Surface tensions of embryonic tissues predict their mutual envelopment behavior. *Development* 1996;122:1611–1620. [PubMed: 8625847]
28. Gardel ML, Nakamura F, Hartwig JH, Crocker JC, Stossel TP, Weitz DA. Prestressed F-actin networks cross-linked by hinged filamins replicate mechanical properties of cells. *Proc. Natl Acad. Sci. USA* 2006;103:1762–1767. [PubMed: 16446458]
29. Gauthier NC, Rossier OM, Mathur A, Hone JC, Sheetz MP. Plasma membrane area increases with spread area by exocytosis of a GPI-anchored protein compartment. *Mol. Biol. Cell* 2009;20:3261–3272. [PubMed: 19458190]
30. Geiger B, Bershadsky A. Assembly and mechano-sensory function of focal contacts. *Curr. Opin. Cell Biol* 2001;13:584–592. [PubMed: 11544027]
31. Ghosh K, Pan Z, Guan E, Ge S, Liu Y, et al. Cell adaptation to a physiologically relevant ECM mimic with different viscoelastic properties. *Biomaterials* 2007;28:671–679. [PubMed: 17049594]
32. Gotsch U, Borges E, Bosse R, Boggemeyer E, Simon M, et al. VE-cadherin antibody accelerates neutrophil recruitment in vivo. *J. Cell Sci* 1997;110:583–588. [PubMed: 9092940]
33. Helmke BP, Goldman RD, Davies PF. Rapid displacement of vimentin intermediate filaments in living endothelial cells exposed to flow. *Circ. Res* 2000;86:745–752. [PubMed: 10764407]
34. Hoffman BD, Crocker JC. Cell mechanics: dissecting the physical responses of cells to force. *Annu. Rev. Biomed. Eng* 2009;11:259–288. [PubMed: 19400709]
35. Hordijk PL, Anthony E, Mul FPJ, Rientsma R, Oomen LCJM, Roos D. Vascular-endothelial-cadherin modulates endothelial monolayer permeability. *J. Cell Sci* 1999;112:1915–1923. [PubMed: 10341210]
36. Hutson MS, Tokutake Y, Chang MS, Bloor JW, Venakides S, et al. Forces for morphogenesis investigated with laser microsurgery and quantitative modeling. *Science* 2003;300:145–149. [PubMed: 12574496]
37. Hutter JL, Bechhoefer J. Calibration of atomic-force microscope tips. *Rev. Sci. Instrum* 1993;64:1868–1873.
38. Isenberg BC, DiMilla PA, Walker M, Kim S, Wong JY. Vascular smooth muscle cell durotaxis depends on substrate stiffness gradient strength. *Biophys. J* 2009;97:1313–1322. [PubMed: 19720019]
39. Juliano RL. Signal transduction by cell adhesion receptors and the cytoskeleton: functions of integrins, cadherins, selectins, and immunoglobulin-superfamily members. *Annu. Rev. Pharmacol. Toxicol* 2002;42:283–323. [PubMed: 11807174]
40. Kasas S, Wang X, Hirling H, Marsault R, Huni B, et al. Superficial and deep changes of cellular mechanical properties following cytoskeleton disassembly. *Cell Motil. Cytoskeleton* 2005;62:124–132. [PubMed: 16145686]
41. Ko KS, Arora PD, McCulloch CA. Cadherins mediate intercellular mechanical signaling in fibroblasts by activation of stretch-sensitive calcium-permeable channels. *J. Biol. Chem* 2001;276:35967–35977. [PubMed: 11466312]
42. Ladoux B, Anon E, Lambert M, Rabodzey A, Hersen P, et al. Strength dependence of cadherin-mediated adhesions. *Biophys. J* 2010;98:534–542. [PubMed: 20159149]
43. Lampugnani MG, Zanetti A, Breviaro F, Balconi G, Orsenigo F, et al. VE-cadherin regulates endothelial actin activating Rac and increasing membrane association of Tiam. *Mol. Biol. Cell* 2002;13:1175–1189. [PubMed: 11950930]

44. Lauffenburger DA, Griffith LG. Who's got pull around here? Cell organization in development and tissue engineering. *Proc. Natl Acad. Sci. USA* 2001;98:4282–4284. [PubMed: 11296276]
45. Levenberg S, Katz BZ, Yamada KM, Geiger B. Long-range and selective autoregulation of Cell–Cell or cell–matrix adhesions by cadherin or integrin ligands. *J. Cell Sci* 1998;111:347–357. [PubMed: 9427683]
46. Lin LAG, Liu AQ, Yu YF, Zhang C, Lim CS, et al. Cell compressibility studies utilizing noncontact hydrostatic pressure measurements on single living cells in a microchamber. *Appl. Phys. Lett* 2008;92:233901–233903.
47. Majno, G.; Joris, I. *Cells, Tissues, and Disease: Principles of General Pathology*. Blackwell Science; Worcester, MA: 1996. p. 974
48. Martens JC, Radmacher M. Softening of the actin cytoskeleton by inhibition of myosin II. *Pflugers Arch* 2008;456:95–100. [PubMed: 18231808]
49. Nelson CM, Chen CS. Cell–Cell signaling by direct contact increases cell proliferation via a PI3K-dependent signal. *FEBS Lett* 2002;514:238–242. [PubMed: 11943158]
50. Nelson CM, Chen CS. VE-cadherin simultaneously stimulates and inhibits cell proliferation by altering cytoskeletal structure and tension. *J. Cell Sci* 2003;116:3571–3581. [PubMed: 12876221]
51. Nelson CM, Pirone DM, Tan JL, Chen CS. Vascular endothelial-cadherin regulates cytoskeletal tension, cell spreading, and focal adhesions by stimulating RhoA. *Mol. Biol. Cell* 2004;15:2943–2953. [PubMed: 15075376]
52. Norman LL, Oetama RJ, Dembo M, Byfield F, Hammer DA, et al. Modification of cellular cholesterol content affects traction force, adhesion and cell spreading. *Cel. Mol. Bioeng* 2010;3:151–162.
53. Oberleithner H, Callies C, Kusche-Vihrog K, Schillers H, Shahin V, et al. Potassium softens vascular endothelium and increases nitric oxide release. *Proc. Natl Acad. Sci. USA* 2009;106:2829–2834. [PubMed: 19202069]
54. Oberleithner H, Riethmuller C, Schillers H, MacGregor GA, de Wardener HE, Hausberg M. Plasma sodium stiffens vascular endothelium and reduces nitric oxide release. *Proc. Natl Acad. Sci. USA* 2007;104:16281–16286. [PubMed: 17911245]
55. Paszek MJ, Zahir N, Johnson KR, Lakins JN, Rozenberg GI, et al. Tensional homeostasis and the malignant phenotype. *Cancer Cell* 2005;8:241–254. [PubMed: 16169468]
56. Rawicz W, Olbrich KC, McIntosh T, Needham D, Evans E. Effect of chain length and unsaturation on elasticity of lipid bilayers. *Biophys. J* 2000;79:328–339. [PubMed: 10866959]
57. Reinhart-King CA. Endothelial cell adhesion and migration. *Methods Enzymol* 2008;443:45–64. [PubMed: 18772010]
58. Reinhart-King CA, Dembo M, Hammer DA. The dynamics and mechanics of endothelial cell spreading. *Biophys. J* 2005;89:676–689. [PubMed: 15849250]
59. Reinhart-King CA, Dembo M, Hammer DA. Cell–Cell mechanical communication through compliant substrates. *Biophys. J* 2008;95:6044–6051. [PubMed: 18775964]
60. Rico F, Roca-Cusachs P, Gavara N, Farre R, Rotger M, Navajas D. Probing mechanical properties of living cells by atomic force microscopy with blunted pyramidal cantilever tips. *Phys. Rev. E Stat. Nonlin. Soft Matter Phys* 2005;72:021914. [PubMed: 16196611]
61. Roca-Cusachs P, Alcaraz J, Sunyer R, Samitier J, Farre R, Navajas D. Micropatterning of single endothelial cell shape reveals a tight coupling between nuclear volume in G1 and proliferation. *Biophys. J* 2008;94:4984–4995. [PubMed: 18326659]
62. Rotsch C, Radmacher M. Drug-induced changes of cytoskeletal structure and mechanics in fibroblasts: an atomic force microscopy study. *Biophys. J* 2000;78:520–535. [PubMed: 10620315]
63. Ryan PL, Foty RA, Kohn J, Steinberg MS. Tissue spreading on implantable substrates is a competitive outcome of Cell–Cell vs. cell–substratum adhesivity. *Proc. Natl Acad. Sci. USA* 2001;98:4323–4327. [PubMed: 11274361]
64. Sato M, Nagayama K, Kataoka N, Sasaki M, Hane K. Local mechanical properties measured by atomic force microscopy for cultured bovine endothelial cells exposed to shear stress. *J. Biomech* 2000;33:127–135. [PubMed: 10609525]

65. Shay-Salit A, Shushy M, Wolfovitz E, Yahav H, Breviario F, et al. VEGF receptor 2 and the adherens junction as a mechanical transducer in vascular endothelial cells. *Proc. Natl Acad. Sci. USA* 2002;99:9462–9467. [PubMed: 12080144]
66. Sneddon IN. The relation between load and penetration in the axisymmetric boussinesq problem for a punch of arbitrary profile. *Int. J. Eng. Sci* 1965;3:47–57.
67. Solon J, Levental I, Sengupta K, Georges PC, Janmey PA. Fibroblast adaptation and stiffness matching to soft elastic substrates. *Biophys. J* 2007;93:4453–4461. [PubMed: 18045965]
68. Stroka KM, Aranda-Espinoza H. Neutrophils display biphasic relationship between migration and substrate stiffness. *Cell Motil. Cytoskeleton* 2009;66:328–341. [PubMed: 19373775]
69. Stroka KM, Aranda-Espinoza H. A biophysical view of the interplay between mechanical forces and signaling pathways during transendothelial cell migration. *FEBS J* 2010;277:1145–1158. [PubMed: 20121945]
70. Svaldo Lanero T, Cavalleri O, Krol S, Rolandi R, Gliozzi A. Mechanical properties of single living cells encapsulated in polyelectrolyte matrixes. *J. Biotechnol* 2006;124:723–731. [PubMed: 16600412]
71. Trepap X, Wasserman MR, Angelini TE, Millet E, Weitz DA, et al. Physical forces during collective cell migration. *Nat. Phys* 2009;5:426–430.
72. Ueki Y, Sakamoto N, Ohashi T, Sato M. Morphological responses of vascular endothelial cells induced by local stretch transmitted through intercellular junctions. *Exp. Mech* 2009;49:125–134.
73. Vinckier A, Semenza G. Measuring elasticity of biological materials by atomic force microscopy. *FEBS Lett* 1998;430:12–16. [PubMed: 9678586]
74. Vitorino P, Meyer T. Modular control of endothelial sheet migration. *Genes Dev* 2008;22:3268–3281. [PubMed: 19056882]
75. Wakatsuki T, Schwab B, Thompson NC, Elson EL. Effects of cytochalasin D and latrunculin B on mechanical properties of cells. *J. Cell Sci* 2001;114:1025–1036. [PubMed: 11181185]
76. Wang N, Stamenovic D. Mechanics of vimentin intermediate filaments. *J. Muscle Res. Cell Motil* 2002;23:535–540. [PubMed: 12785103]
77. Wang N, Tolic-Norrelykke IM, Chen J, Mijailovich SM, Butler JP, et al. Cell prestress. I. Stiffness and prestress are closely associated in adherent contractile cells. *Am. J. Physiol. Cell Physiol* 2002;282:C606–C616. [PubMed: 11832346]
78. Waterman-Storer CM, Salmon WC, Salmon ED. Feedback interactions between Cell–Cell adherens junctions and cytoskeletal dynamics in Newt lung epithelial cells. *Mol. Biol. Cell* 2000;11:2471–2483. [PubMed: 10888682]
79. Weisenhorn AL, Khorsandit M, Kasast S, Gotzost V, Butt H-J. Deformation and height anomaly of soft surfaces studied with an AFM. *Nanotechnology* 1993;4:106–113.
80. Yeung T, Georges PC, Flanagan LA, Marg B, Ortiz M, et al. Effects of substrate stiffness on cell morphology, cytoskeletal structure, and adhesion. *Cell Motil. Cytoskeleton* 2005;60:24–34. [PubMed: 15573414]
81. Zhu AJ, Watt FM. Expression of a dominant negative cadherin mutant inhibits proliferation and stimulates terminal differentiation of human epidermal keratinocytes. *J. Cell Sci* 1996;109:3013–3023. [PubMed: 9004036]

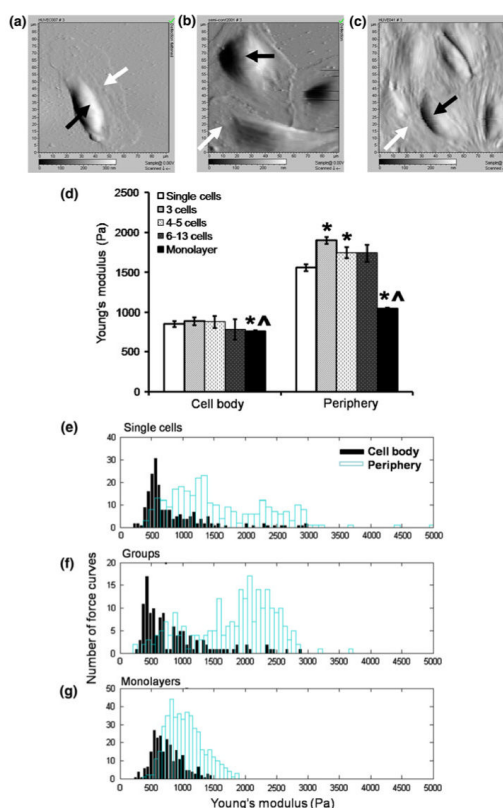
**FIGURE 1.**

(A) Example of a force vs. distance curve obtained by atomic force microscopy (AFM). Prior to contact between the AFM tip and the sample (a) there is no deflection of the laser. Once the tip has contacted the sample (b), the laser begins to deflect as the sample is indented (c). (B) Deflection vs. distance data were fit using the Hertz–Sneddon model (see Materials and Methods). The point of contact was chosen when the slope became nonzero (approximately 50 pN/nm after converting to force vs. distance), while the final indentation was chosen to be about 250 nm. In the case of a very stiff sample, the deflection (or force) rises sharply with distance. Curves are shown for a soft location (i.e., cell body) and a relatively stiff location (i.e., periphery). (C) Young's modulus of single cells at the cell body and periphery locations (see Fig. 3a for clarification) at both room temperature (23 °C) and 37 °C with 5% CO<sub>2</sub> and 55% humidity. No significant differences were measured between these conditions using our experimental set-up.



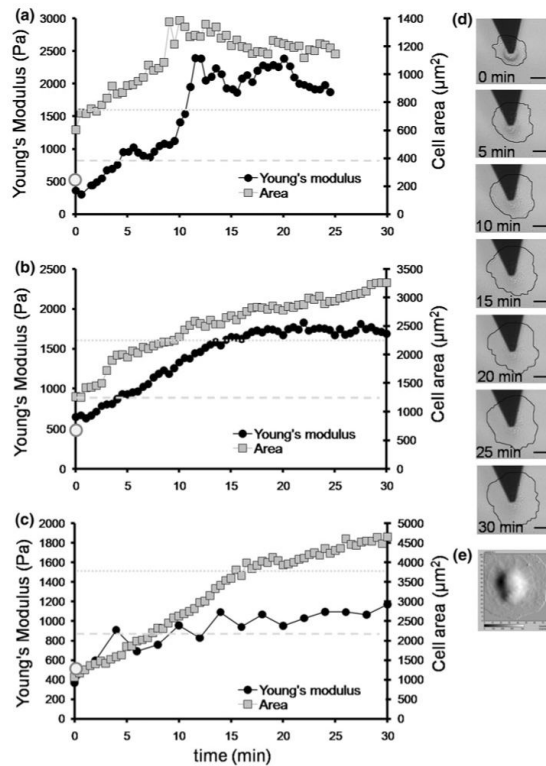
**FIGURE 2.**

(a) Cellular area as a function of degree of Cell–Cell contact on fibronectin-coated glass substrates. Bars indicate mean of  $N$  cells, while error bars indicate standard error.  $N$  equals 167, 249, and 192 for single cells (S), groups (G), and monolayers (M), respectively. \* indicates  $p < 0.05$  with single cells, while ^ indicates  $p < 0.05$  with monolayers using Student's  $t$  test. Also shown are phase contrast images of (b) a single cell, (c) four cells in contact, and (d) a monolayer of cells. Scale bars are  $20\ \mu\text{M}$ .



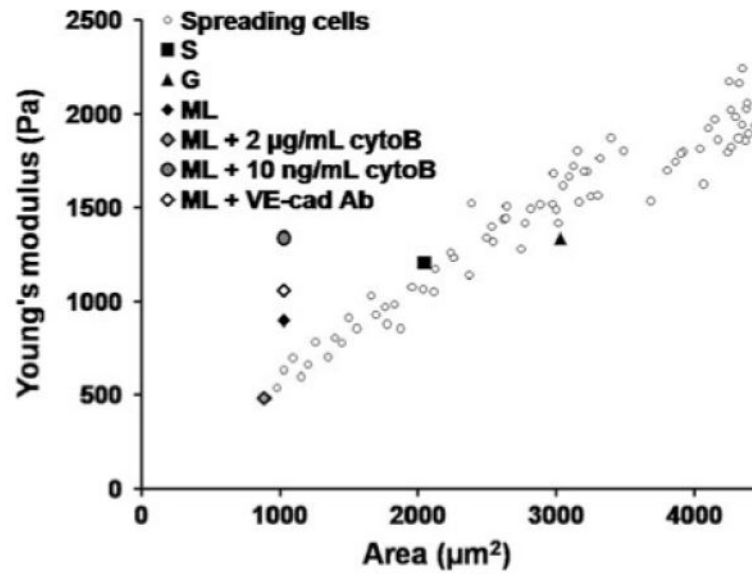
**FIGURE 3.**

Atomic force microscopy contact deflection images of (a) a single control endothelial cell, (b) 3 cells in contact, and (c) a monolayer of cells. Image size is  $90\ \mu\text{M} \times 90\ \mu\text{M}$ . Black arrows point to examples of cell body locations, while white arrows point to examples of periphery locations. (d) Young's modulus of cells for the cell body and periphery locations as a function of Cell-Cell contact. Bars indicate mean of  $N$  force curves per condition, while error bars indicate standard error. \* indicates  $p < 0.05$  with single cells at the same location, while ^ indicates  $p < 0.05$  with groups of 3 cells at the same location using a Student's  $t$  test. For all locations, the periphery region is stiffer than the cell body region ( $p < 0.05$ ).  $N = 195, 44, 67, 16, 246$  for single cells, groups of 3 cells, groups of 4-5 cells, groups of 6-13 cells, and monolayers, respectively, at the cell body location.  $N = 284, 100, 98, 46, 457$  for single cells, groups of 3 cells, groups of 4-5 cells, groups of 6-13 cells, and monolayers, respectively, at the periphery location. Also shown are distributions of Young's moduli for (e) single cells ( $N = 195$  for cell body and  $N = 284$  for periphery region), (f) all groups of cells ( $N = 127$  for cell body and  $N = 244$  for periphery region), and (g) monolayers ( $N = 246$  force curves for cell body and  $N = 457$  force curves for periphery region).



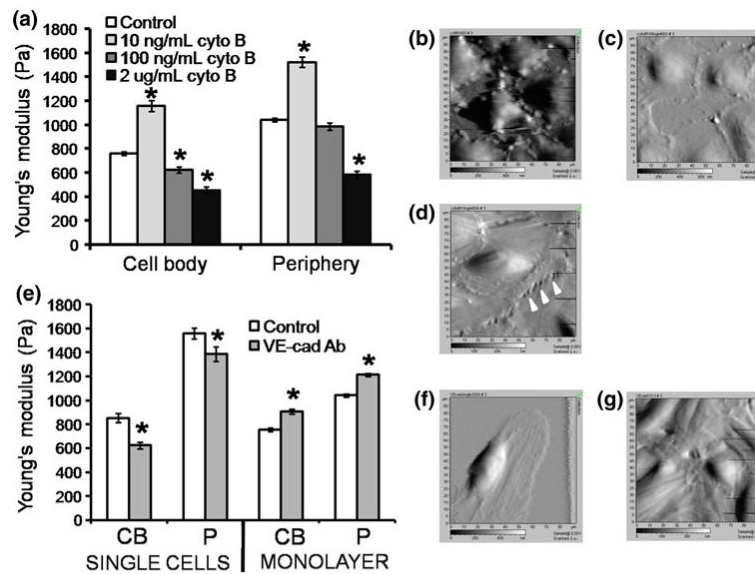
**FIGURE 4.**

Young's modulus and cell area vs. time are overlaid on the same plot for three representative spreading cells. A time of  $t = 0$  indicates the time at which measurements began; typically this was 15–30 min after plating. Shown are plots for three different representative cells, with AFM measurements taken every 30 s (a, b) or every 2 min (c). Gray outlined dot at  $t = 0$  indicates typical Young's modulus of cytochalasin B-treated cells. Gray large dashed line and gray small dashed line indicate typical Young's modulus of control single cells at the cell body and periphery locations, respectively. (d) Time-course sequence of spreading cell from (b). These images show the AFM cantilever positioned over the cell during spreading. The cantilever remained stationary during the course of spreading. In each image cells have been outlined in black by hand to help with cell visualization. Scale bar is  $20 \mu\text{M}$  for all images. (e) AFM deflection image of cell from (c) after it has completely spread. Image size is  $90 \mu\text{M} \times 90 \mu\text{M}$ .



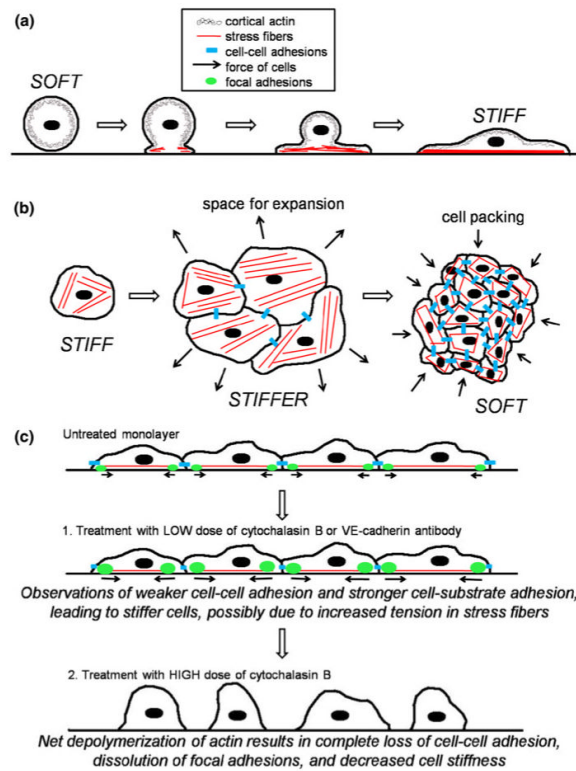
**FIGURE 5.**

Young's modulus vs. area for  $N = 8$  spreading cells (white outlined circles). Also shown are the average (area, stiffness) of single cells (S), groups (G), monolayers (ML), and monolayers treated with VE-cadherin antibody (VE-cad Ab) or cytochalasin B (cytoB). In all cases, the stiffness plotted is the average stiffness of the cell body and periphery regions.

**FIGURE 6.**

Mean Young's modulus for (a) cytochalasin B (cytoB)-treated cells and (e) VE-cadherin antibody-treated cells at the cell body and periphery locations. Bars indicate mean of  $N$  force curves, while error bars indicate standard error. \* indicates  $p < 0.05$  with control at same location using Student's  $t$  test.  $N = 246, 241,$  and  $70$  for control, VE-cadherin antibody-treated, and cytoB-treated cells, respectively, at the cell body (CB) location.  $N = 457, 583,$  and  $22$  for control, VE-cadherin antibody-treated, and cytoB-treated cells, respectively, at the periphery (P) location. Also shown are atomic force microscopy contact deflection images of HUVEC monolayers treated with (b)  $2 \mu\text{g}/\text{mL}$  cytoB, (c)  $100 \text{ ng}/\text{mL}$  cytoB, and (d)  $10 \text{ ng}/\text{mL}$  cytoB. White arrowheads in (d) point to tether-like structures at Cell-Cell junctions. Also shown are (f) single cells and (g) monolayers, both treated with a VE-cadherin antibody. AFM image size is  $90 \mu\text{M} \times 90 \mu\text{M}$ .



**FIGURE 8.**

Schematic which summarizes our observations of spreading cells and cells with varying degrees of Cell–Cell contact. (a) Prior to developing adhesions with the underlying substrate, the cell contains a layer of cortical actin beneath the membrane. This cortical actin network is soft compared with the parallel bundles of F-actin filaments (stress fibers) which polymerize and crosslink during spreading. Upon touching down on the substrate, the cell begins to adhere to the surface and actin polymerizes, causing the cell to extend outward onto its substrate. When it is fully spread, there exists a dense network of stress fibers which extend into the periphery of the cell, while a layer of cortical actin still remains. As the stress fibers contract, tension in the entire cell, including the cell body region, is increased. This generates the increased stiffness of the cell. (b) In the transition from a single cell to a network, the cells develop Cell–Cell contacts composed of numerous adhesion proteins. Because the cells have space around them to move, they likely extend outward through actin polymerization, while (visibly) still maintaining Cell–Cell contacts. Increased focal adhesion size at this point suggests that tension in the cell has increased, leading to increased cell stiffness. As more and more cells enter the group, they begin packing and eventually form a monolayer. Note that in our schematic cartoon, the monolayer continues outward infinitely in all directions; pictured are cells at the interior. Here, the stress fibers are arranged mainly around the periphery of the cell, suggesting that cell packing forces have caused rearrangement of F-actin, possibly resulting in softer cells. In a monolayer, there are less focal adhesions per area, indicating that cell–substrate adhesion has decreased, but likely Cell–Cell adhesion has increased. The actin is linked to the cellular junctions through VE-cadherin, and the VE-cadherin molecules on neighboring cells link to each other, creating a physical link between cells through which force can be transferred. (c) Once in a monolayer, treatment with VE-cadherin antibody or a low dose of cytochalasin B presumably weakens Cell–Cell adhesions. Prior to treatment, the cells have some degree of Cell–Cell adhesion and cell–substrate adhesion. After treatment to weaken Cell–Cell adhesions, the cells

develop stronger cell–substrate adhesions (larger focal adhesions), leading to increased tension, and thus increased stiffness, in the cells. If the monolayer is instead treated with a high dose of cytochalasin B, there is a complete loss of Cell–Cell adhesion, dissolution of focal adhesions, and decrease in cell stiffness due to the net depolymerization of actin filaments.